ADVANCED FUNCTIONAL MATERIALS
www.afm-journal.de

Materials Views
www.MaterialsViews.com

p-Type Beta-Silver Vanadate Nanoribbons for Nanoelectronic Devices with Tunable Electrical Properties

*Mei Feng, Lin-Bao Luo, Biao Nie, and Shu-Hong Yu**

β-$AgVO_3$, as a stable phase and a typical silver vanadium oxide, has performed special ionic and electrical properties. The construction of nanoelectronic devices based on ultralong β-$AgVO_3$ nanoribbons (NRs) is reported, including nano-field-effect transistor (nano-FET) and nano-Schottky barrier diode (nano-SBD). Owing to the specific channel structure and ion conductivity, the nano-FET exhibits typical p-type semiconductor characteristics and the nano-SBD with Al contacts performs a prominent rectifying behavior with an on/off ratio of up to 10^3. Besides, tunable electrical transport properties can be achieved by tailoring the material properties, and it is demonstrated that the bridging NR numbers and diameters have a positive effect on electrical transport properties, while a complex variation trend is observed in the case of surface modification by photo-irradiation. Electron spin resonance (ESR) spectrum further illuminates that the induced vacancies play an important role on the electrical transport properties of β-$AgVO_3$ nanoribbons. Easy access to the ultralong β-$AgVO_3$ NRs makes them a promising candidate for potential applications in nanoelectronic devices.

1. Introduction

Nanostructured electronic devices have inspired much effort to facilitate the continuing miniaturization of electronic devices.[1] As a basic building block for diverse nanodevices applications, such as integrated circuits, displays, and memory devices, field-effect transistors based on semiconductor nanostructures (nano-FETs) have played a core role in the field of nanometer-scale electronics.[2–4] In particular, nano-FETs based on one-dimensional nanostructures, such as nanowires (NWs) and nanoribbons (NRs) are getting increasing interest.[5–9] In addition, as required by the assembly and integration of 1D nanodevices, the well developed 1D p-type semiconductors have promoted more opportunities for various nanoscale electronics.[10–12] By this token, tremendous efforts have been made to produce p-type semiconductor nanostructures. The most common way, for example, is to introduce a defect level (acceptor level) slightly above the valance band by incorporating impurity atoms into the nanostructures.[1,13] However, the nanostructures obtained in this way always unfortunately present poor stability and reproducibility, which greatly hinders their device application.[10]

Recently, one-dimensional silver vanadium oxides (SVO) with typical p-type conduction behavior and a wide band gap,[14–17] have attracted much interest for their potential applications in catalysis,[18,19] surface-enhanced Raman scattering (SERS) substrates,[20] conducting and optoelectronic materials,[17,19,21] owing to their unique channel structure and ionic properties.[17,22,23] β-$AgVO_3$, as a stable phase of SVO compounds, has been prepared by many methods.[15,17,24] In spite of this progress, to the best of our knowledge, the electrical property of p-type nano-FETs based on 1D β-$AgVO_3$ has rarely been investigated yet. On the other hand, to promote their further applications in various electronic nanodevices, it has become an urgent task to understand and control the electrical transport properties of these p-type semiconductors, especially their interaction with metal contacts and tunable electrical properties. Nano-Schottky barrier diodes (nano-SBDs) can exhibit high performance in many areas.[25–28] However, Al/β-$AgVO_3$ nano-Schottky diodes have not been fabricated and investigated yet.

Herein, we examine the electrical properties of individual β-$AgVO_3$ nanoribbons by constructing nano-FETs. The nano-FET showed typical gating effect, with a p-type electrical conduction behavior. The Schottky-junction diode made of a single NR and Al contacts with stable device performance has been investigated as well. To explore more scalable potential applications in future electronic nanodevices, we finally studied the bridging NR numbers, diameters and photo-irradiation duration dependent electrical properties of β-$AgVO_3$ NRs.

2. Results and Discussion

The elegant β-$AgVO_3$ NRs were synthesized through a hydrothermal route reported previously (see Supporting Information).[15] The morphology and dimensions of the as-prepared

M. Feng, Prof. S.-H. Yu
Division of Nanomaterials and Chemistry
Hefei National Laboratory for Physical Sciences at Microscale
Department of Chemistry
University of Science and Technology of China
Hefei, Anhui 230026, China
E-mail: shyu@ustc.edu.cn
Prof. L.-B. Luo, B. Nie
Anhui Provincial Key Laboratory of Advanced Functional Materials and Devices
School of Electronic Science and Applied Physics
Hefei University of Technology
Hefei, Anhui 230009, China

DOI: 10.1002/adfm.201300413

 © 2013 WILEY-VCH Verlag GmbH & Co. KGaA, Weinheim

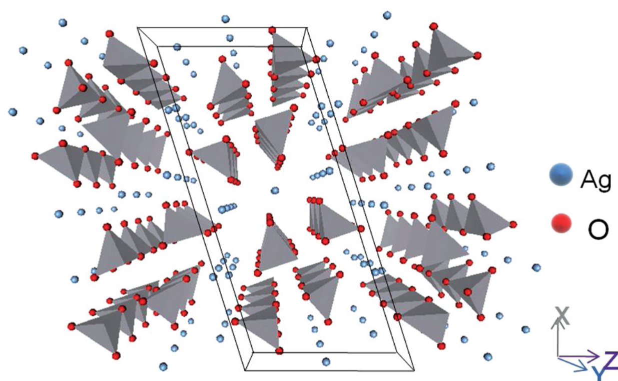

Figure 1. Perspective view of the channel structure (1 × 3 × 3 cells) for β-$AgVO_3$, red balls, O atoms; blue balls, Ag atoms.

nanomaterials were investigated by scanning electron microscopy (SEM), transmission electron microscopy (TEM) and high-resolution transmission electron microscopy (HRTEM), via which ultralong SVO NRs on a large scale with lengths of at least tens of micrometers and diameters of 100–600 nm can be easily visualized (Supporting Information, Figure S1a–c). Interestingly, silver nanoparticles will readily appear on the NRs surface when the sample is under long-time bombardment of high-energy electrons (Supporting Information, Figure S1c). The phase and purity of the as-prepared nanomaterials were characterized by the X-ray diffraction (XRD) (Supporting Information, Figure S1d) and all the diffraction peaks have been indexed as β-$AgVO_3$ (JCPDS card 29-1154).[15]

As an important narrow band gap (<3.0 eV) semiconductor in silver-based oxides, β-$AgVO_3$ NRs have been utilized in many advanced nanodevices,[29,30] by virtue of their novel electrical transport properties resultant from its special structure and ionic properties. **Figure 1** shows the perspective view of the channel structure of β-$AgVO_3$ NRs in which different types of silver ions were located in different positions. To further elucidate the special structural feature of this material, we provide another schematic illustration in Figure S2a, Supporting Information. Obviously, the silver ions were sandwiched between the lamellar vanadate layers. Such a crystallographic with cations existing between separate layers can allow their easy motion within the layer.[23] Therefore, it is rational that our β-$AgVO_3$ NRs will perform good electrical properties owing to the movement of Ag^+ cations in the layer. As a matter of fact, this assumption was experimentally verified by the electrical conductivity analysis. Figure S2b, Supporting Information, plots a typical *I–V* curve of the individual β-$AgVO_3$ NR under bias voltages from –10 V to 10 V. Based on this, the conductivity value of the NR was calculated to be about 7.53×10^{-2} S cm^{-1}, which is in accordance with that in a previous study.[15] These results further guaranteed their outstanding applications in electrical nanodevices.

To further assess the electrical transport properties of the as-prepared β-$AgVO_3$ NRs, individual NR-based FET device was constructed. **Figure 2**a illustrates the detailed device fabrication process (see Supporting Information). Briefly, well-defined NRs were stochastically dropped onto a SiO_2 (300 nm)/p^+-Si substrate, and then Cu/Au source and drain electrodes were defined on the dispersed NRs by photolithography, followed by electron-beam evaporation and lift-off process. During the device characterization, the underneath heavily doped Si substrate will sever as the global back gate in the FETs. As to nano-Schottky barrier diodes (nano-SBDs), the deposited Al layer was utilized as Schottky contact electrode between the two adjacent Cu/Au electrodes.

The electrical characteristics of the back-gate nano-FET are shown in Figure 2b,c. Figure 2b exhibits the source-drain current (I_{DS}) versus source-drain voltage (V_{DS}) curves, which were measured under varied gate voltage (V_G) from –40 to 20 V at a step of 15 V. The obvious linear curves insinuate that ohmic contact formed between the electrodes and the nanostructures. In addition, it is interesting to note that the conductance of the NR monotonously increases with the augment of V_{GS}, signifying the p-type conduction behavior of β-$AgVO_3$ NR. As found in previous work,[31,32] a spot of nanoscale Ag can be engendered by resistively heating when applying voltage. Consequently, some vacancies ($Ag_{Ag}^{\times}$ and $V_O^{\cdot\cdot}$) would come into being at the same time (Supporting Information, Figure S3), and the formation process can be described as the following equations:

$$\overset{\times}{Ag} + e \longrightarrow Ag_{Ag}^{\times} \quad (1)$$

$$O_O^{\times} \longrightarrow 1/2 O_2 + V_O^{\cdot\cdot} + 2e \quad (2)$$

In this case, we proposed that the introduction of acceptor-like defect level by these vacancies would contribute to accumulation of holes gas within the nanostructure, which exhibited the p-type behavior. Figure 2c shows the transfer characteristic curves at $V_{DS} = 10$ V. The hole carrier mobility can be obtained by employing two dots (I and II) in the linear region of the source-drain current versus the threshold gate voltage (I_{DS}–V_G) curve, according to the equations as below:

$$g_m = \left| dI_{DS}/dV_G \right| \quad (3)$$

$$\mu_h = g_m / (Z/L)\, C_0\, V_{DS} \quad (4)$$

$$p = 1/\rho\, q\, \mu_h \quad (5)$$

where Z/L is the width-to-length ratio of the channel. The capacitance per unit area is given by $C_0 = \varepsilon\varepsilon_0/h$, where ε is the dielectrical constant of SiO_2 (3.9) and h is the SiO_2 thickness (500 nm). On the basis of these values, the transconductance (g_m) of the NR was calculated to be about 0.136 nS and the hole carrier mobility (μ_h) was 0.505 $cm^2\ V^{-1}\ s^{-1}$. In addition, the hole carrier concentration (n) can be estimated as 3.37×10^{12} cm^{-3} from Equation 5.

To study the electrical transport characteristics of individual-NR-based SBD shown in Figure 2d, two parallel Cu/Au ohmic contact electrodes were first defined and then one Al electrode was deposited between the Cu/Au electrodes. Figure 2e exhibits the representative *I–V* curve of a NR SBD at room temperature. Notably, one can see that Al/β-$AgVO_3$ NR SBD reveals an excellent rectification characteristic; namely, it can allow an electric current to pass in one direction, while blocking current in the

© 2013 WILEY-VCH Verlag GmbH & Co. KGaA, Weinheim

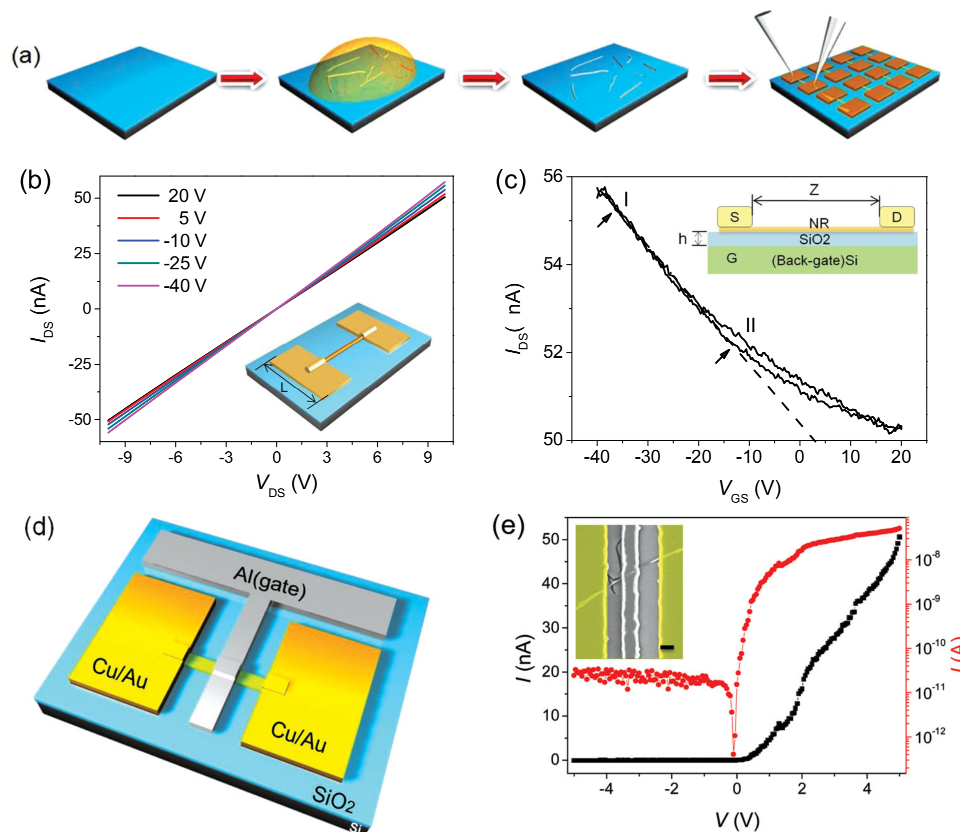

Figure 2. a) Schematic illustration for fabrication of the individual β-$AgVO_3$ NR nanodevices. b) The I_{DS}–V_{DS} curves of the individual β-$AgVO_3$ NR bottom-gate nano-FET; inset shows the schematic device configuration of the nano-FET. c) The I_{DS}-V_G curve of the nano-FET. Note: I and II were two dots indicated by arrows in the linear region of the curve, which were chosen to estimate the hole mobility. The coordinates were (–36 V, 52.18 nA) and (–13 V, 55.35 nA), respectively. Inset illuminated almost all parameters in the back- gate nano-FET. d) Schematic illustration for the fabricated β-$AgVO_3$ NR SBD, both Al and Cu/Au electrodes have been shown. e) *I–V* characteristic of the nano-SBD based on an individual β-$AgVO_3$ NR, inset shows a typical SEM image of the NSBD with artificial colors; the scale bar is 5 µm.

opposite direction. Specifically, the leakage current is less than –0.8 nA at a reverse bias of up to –5 V. Further analysis yields a rectification ratio of up to $\approx 10^3$ in the range from –5 to 5 V and the turn-on voltage of ≈0.5 V. As for an ideal diode, the *I–V* characteristic of a Schottky diode can be described by the following equations:[26]

$$I = I_0[\exp(qV/nkT) - 1] \quad (6)$$

$$I_0 = AA^* T^2 \exp(-(q\Phi_{Bn}/kT)) \quad (7)$$

where I_0 is the reverse saturation current, n the ideality factor, A^* effective Richardson's constant, A the Schottky constant area, q the electronic charge, k the Bolzmann's constant, T the temperature in kelvins and Φ_{Bn} the barrier height. By fitting the *I–V* curve with Equation 4, n was finally derived to be ≈1.957. Moreover, analogous fitting of Equation 5 can yield a Φ_{Bn} of ≈0.485 eV. Here, it should be mentioned that the relatively high ideality factor and low barrier height is probably associated with the threshold voltage drop across an interfacial layer, which has been formed between Al electrode and the β-$AgVO_3$ NR during the Al deposition process. Another factor that contributes to such non-ideal *I–V* characteristics is interface states. Due to the low fabrication temperature, a huge amount of surface state, including dangling bond, surface defect will be formed. They can behave as efficient recombination centers to support the trap-assisted tunneling currents and finally give rise to the high n, increased reverse current, and low Φ_{Bn}.[33]

The above results demonstrated that the single NR based nano-FET exhibited well-defined p-type conduction. What is more, by connecting the single NR with asymmetric electrodes, a SBD device with obvious revivifying behavior can be also fabricated. In the following part, we would like to explore how the NR diameters will influence the electrical conductive properties. This issue is worth studying in that diameters dependent device performance have already been reported in various devices, for example, nano-FET, gas and pH sensors,[34–37] nanobiosensors,[38] and photodetector and transparent conducting films,[39] especially electrical transport properties.[40] **Figure 3**a shows the *I–V* characteristics of various NRs with increasing diameters of 400, 900, 2600, and 6300 nm, corresponding to the SEM images in Figure 3b–e, respectively. It was clear that the electrical conductivity (EC) of β-$AgVO_3$ NRs has exhibited a positive correlation with the NR diameters. In other words, the wider the NRs, the higher the EC will be. This feature is important as it allows us to accurately control the electrical property by simply adjusting the diameter of the nanostructures.

© 2013 WILEY-VCH Verlag GmbH & Co. KGaA, Weinheim

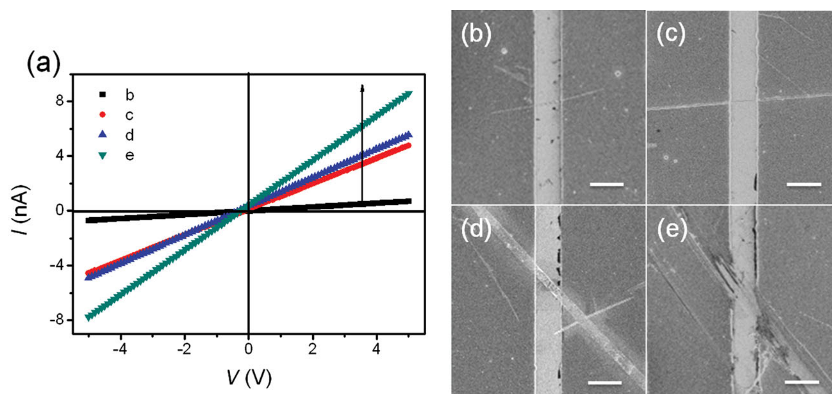

Figure 3. a) Diameter dependent *I–V* curves of β-$AgVO_3$ NRs. b–e) SEM image of NRs with diameters of 400, 900, 2600, and 6300 nm, respectively. The scale bar is 10 µm.

Based on the above observation and analysis, we reckoned that devices with more NRs should be more stable and conductive. Though the underlying mechanism hasn't been explored, we conferred that the phenomena should be owing to the junctions and overlapping between NRs.[13] As a result, we believe that β-$AgVO_3$ NR-based thin film devices should have stable signals and might be practically used as building blocks in the future electronics devices. To be noticed, when comparing the *I–V* curves of NRs with and without photo-irradiation treatment in Figure 4f,g, we observed enhanced electrical conductivities of devices with same bridging numbers and deduced that the photo-irradiation can also have an effect on the EC for electrical devices.[43,44]

In addition, we also examined the electrical property of the devices constructed by multiple nanoribbons which would be the most promising building blocks for future electronic devices application.[41,42] Several nanodevices with gradually increamental NR numbers have been fabricated, as illuminated in the SEM images (Supporting Information, Figure S4). The magnified SEM images in **Figure 4** show that the almost uniform bridging NRs were separated from each other; and the bridging numbers have been chosen as 1, 2, 4, 5 and multiple (n), respectively. The bridging numbers in the multiple-nanoribbon device (Figure 4e) were speculated to be more than 50 by rough estimatation. Correspondingly, Figure 4f exhibits the *I–V* curves of the bridging NRs. Apparently, when augmenting the bridging numbers, the electrical conductivity of the NRs increased obviously. Noticeably, the *I–V* curve with a great many of bridging numbers (>50) have deviated far away from others. For intuitionistic analysis, we have set up a series of linear fitting curves and approximately estimated the EC values of these devices (Supporting Information, Figure S5). The results illuminated that the device with multiple bridging numbers have exhibited higher electrical conduction than that with less nanoribbons.

Interestingly, when the nanoribbons were shinned with photo-irradiation for 60 min under modeling sunlight from a 300 W Xe lamp, great change in their conductivity would takes place. Figure 4g exhibits the *I–V* characteristics of 60-min irradiated β-$AgVO_3$ NRs. Clearly, for all devices with various numbers of NRs, their electrical conductivities are found to increase after light illumination. Besides, taking the linear fitting into consideration, we speculated that the EC value of the device with multiple bridging numbers should be at least 4 times higher than others (Supporting Information, Figure S6).

Next, we examined evolution of the electrical conductivity as a function of photo-irradiation duration. To make the electrical measurement more reliable, only devices with 2 and multiple bridging numbers were considered. **Figure 5**a,b

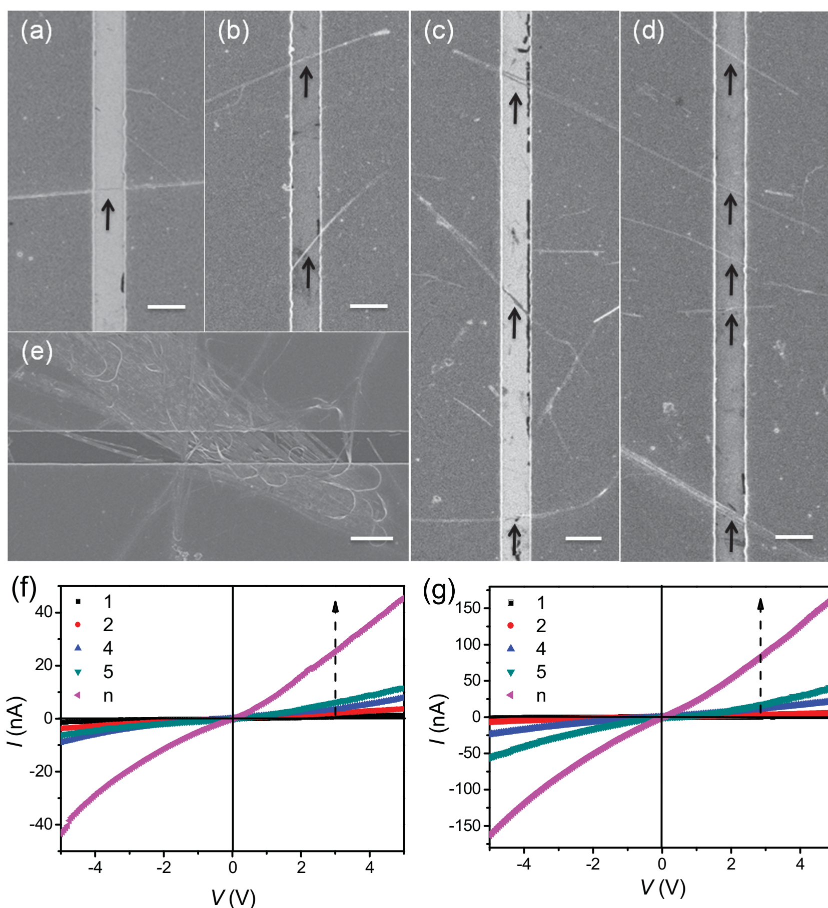

Figure 4. SEM images of β-$AgVO_3$ NRs with a) 1, b) 2, c) 4, d) 5, and e) multiple (>50) bridging numbers, as well as the bridging number dependent *I–V* curves under photo-irradiation time for f) 0 min and g) 60 min, respectively. Note: black dash lined arrows in the SEM images indicate the location of the bridging nanoribbons. The scale bars is 10 µm.

© 2013 WILEY-VCH Verlag GmbH & Co. KGaA, Weinheim

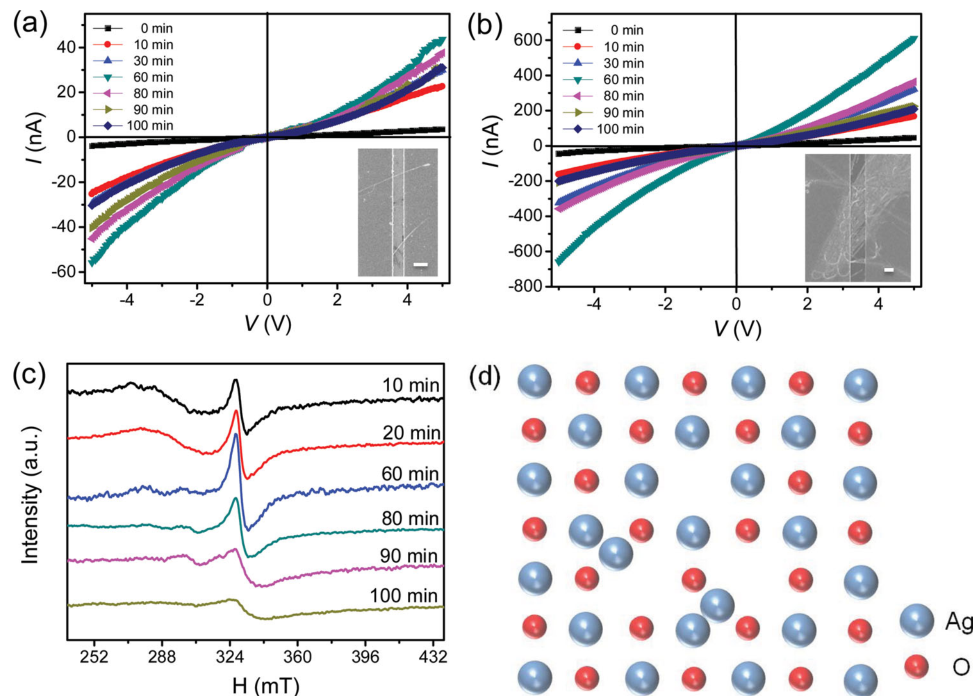

Figure 5. Photo-irradiation time dependent *I–V* curves of the devices with a) 2 and b) multiple NRs. Insets display the corresponding SEM images of devices. The scale bars is 10 µm. c) The ESR spectra of the β-$AgVO_3$ NRs with increasing photo-irradiation time. d) Ichnographyic schematic illustration for the formation of silver and oxygen vacancies (V_{Ag}^- and V_O^{2+}).

showed the corresponding *I–V* characteristics under light illumination for 0, 10, 30, 60, 80, 90, and 100 minutes. When the device composed of 2 NRs was irradiated for 10 min, the current increased by 80% percent. With time further augmenting, the current increased correspondingly. Nevertheless, when the device was irradiated for more than 60 min, the current by contrast began to decrease sharply, independent of further augment in irradiation duration. This decrease in current was even observed when irradiated for more than 100 min. Similar current variation was observed for device composed of many a NRs (>50) as well. As we discussed latter, such a photo irradiation dependent current evolution should be associated with the formation silver nanoparticles on the backbone of NRs (Supporting Information, Figure S7).

To unveil the physical origin behind this variation, we have analyzed the electron spin resonance (ESR) spectra of these NRs corresponding to different photo-irradiation times shown in Figure 5c. Interestingly, the resonance signal was observed to get stronger at first in the range of 0–60 min, and then became weaker with the increase of photo-irradiation time, in good consistence with the current variations (Figures 5a,b). In light of this agreement, we speculate that photo-irradiation can induce the in situ formation of silver NPs on the backbones of β-$AgVO_3$ NRs. The reaction mechanism before 60-min photo-irradiation mainly involved Equations 1,2, via which silver and oxygen vacancies ($Ag_{Ag}^{\times}$ and $V_O^{\cdot\cdot}$) contributing to the ESR signals came into being on the backbones of β-$AgVO_3$ NRs (Figure 5d). According to previous studies,[45–47] the surface defects via surface engineering can influence the electrical properties of transition-metal oxides and thus provide alternative strategies for controlling the device performance. On the contrary, the weakened EC and ESR intensities after photo-irradiation for more than 60-min time should be ascribed to the gradual vanish of vacancies. Thus, we deduced that some vacancies would be consumed in the subsequent process; and at the same time silver oxides would come into being.[48,49] Therefore, a pellucid schematic illustration for these whole processes can be depicted in **Figure 6**, in which silver and silver oxide nanoparticles formed on the backbones of β-$AgVO_3$ NRs sequentially. To verify the appearance of silver and silver oxide nanoparticles, we have shined the nanoribbons by photo irradiation for 100 min. The morphology and phase purity of the photo-irradiated nanoribbons and the particles were characterized by TEM, HRTEM and XRD, respectively. Clearly, TEM image showed the formation of particles on the surface of nanoribbons (Supporting Information, Figure S8a), and HRTEM images displayed the lattice spacings of these marked particles, which corresponded well with silver and silver oxides nanoparticles (Supporting Information Figure S8b,c). Moreover, XRD patterns of the nanoribbons under photo irradiation for 0 and 100 min further confirmed the formation of these nanoparticles (Supporting Information, Figure S8d).

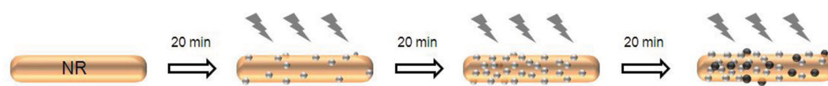

Figure 6. Schematic illustration for the formation of nanoparticles on the nanoribbon surface. Note: gray ball, silver nanoparticles; black ball, silver oxide nanoparticles.

© 2013 WILEY-VCH Verlag GmbH & Co. KGaA, Weinheim

3. Conclusions

In summary, we report the construction of nanoelectronic devices based on the elegant β-$AgVO_3$ NRs, such as nano-FETs and nano-SBDs. Typical p-type electrical behavior and stable device performance on the interaction with Al contacts have been observed. In addition, by tailoring the diameter of the bridging NRs and their numbers, and even the surface modification through light-irradiating the backbones of NRs, tunable electrical transport properties can be achieved. It is expected that this kind of conductive β-$AgVO_3$ NRs may act as a promising candidate for application in the future electronic devices.

4. Experimental Section

Chemicals: All the chemicals were of analytical grade, commercially available from Shanghai Chemical Reagent Co. Ltd. (P. R. China), and used without further purification.

Material and Preparation: The synthesis of 1D ultralong β-$AgVO_3$ was based on the procedure reported recently. In a typical procedure of synthesizing β-$AgVO_3$, 0.0765 g of $AgNO_3$, 0.0818 g of V_2O_5, and 40 mL of distilled were mixed together in a Teflon-lined stainless-steel autoclave with a volume capacity of 50 mL. Then 2 mL of pyridine was also dropwise added into the autoclave under vigorous stirring. The mixed solution displayed a color-change from brick red to light yellow when pyridine is injected. After 30 min, the reaction mixture formed a homogeneous yellow suspension. The autoclave was sealed and maintained at 180 °C for 3 h, then cooled to room temperature naturally. The obtained gel state pale yellow solids, which overflowed the all inner lining, were collected by centrifuging the reaction mixture; the products were then washed with distilled water and absolute ethanol several times each and dried in a vacuum at 60 °C for 6 h for further characterization.

Characterization: The phase purity of the obtained samples was characterized by X-ray diffraction (XRD), which was carried out on a Philips X'Pert PRO SUPER X-ray diffractometer equipped with graphite monochromatized Cu Ka radiation ($\lambda = 1.541874$ Å). The morphologies of the as-prepared products were observed by scanning electron microscopy (SEM), transmission electron microscopy (TEM), and high-resolution transmission electron microscopy (HRTEM). SEM was carried out with a field emission scanning electron microanalyzer (JEOL-6700F). TEM and HRTEM were performed on JEOL-2010 operated at an acceleration voltage of 200 kV.

Device Construction and Measurements: To make electrical contact with requisite NRs, diluted aqueous suspension of NRs were stochastically dropped and dried on SiO_2 (300 nm)/p^+Si substrates respectively at first. For back-gate nano-FET, the source and drain double-layer electrodes (Cu 40 nm/Au 60 nm) were defined by a photolithography and electron-beam evaporation process. Finally, the remaining photoresist was stripping by acetone soaking. The nano-SBD was constructed by the same disperse and two photolithography processes. The second deposited Al layer was utilized as Schottky contact electrode between the two adjacent first deposited Cu/Au electrodes by electron-beam evaporation method. Electrical measurements were carried out at room temperature by using a semiconductor characterization system (Keithley 4200). The spacing intervals among gold contacts are 10 µm. The photo-irradiation treatment was performed under modeling sunlight from a 300 W Xe lamp.

Supporting Information

Supporting Information is available from the Wiley Online Library or from the author. It includes: SEM, TEM and HRTEM images, XRD patterns, perspective view, *I–V* curve, linear fitting curves and estimation of the EC values, schematic illustration.

Acknowledgements

M.F. and L.-B.L. contributed equally to this work. The authors acknowledge the special funding support from the National Basic Research Program of China (Grant 2010CB934700), the National Natural Science Foundation of China (Grants 91022032, 91227103, 21101051), the Ministry of Science and Technology of China (Grant 2012BAD32B05-4), the Chinese Academy of Sciences (Grant KJZD-EWM01-1), the Fundamental Research Funds for the Central Universities (2012HGCX0003, WK 2060190021), and the Principal Investigator Award by the National Synchrotron Radiation Laboratory at the University of Science and Technology of China.

Received: February 1, 2013
Revised: March 12, 2013
Published online: May 27, 2013

[1] J. S. Lee, S. N. Cha, J. M. Kim, H. W. Nam, S. H. Lee, W. B. Ko, K. L. Wang, J. G. Park, J. P. Hong, *Adv. Mater.* **2011**, *23*, 4183.
[2] Q. Y. He, S. X. Wu, Z. Y. Yin, H. Zhang, *Chem. Sci.* **2012**, *3*, 1764.
[3] J. A. del Alamo, *Nature* **2011**, *479*, 317.
[4] J. P. Colinge, C. W. Lee, A. Afzalian, N. D. Akhavan, R. Yan, I. Ferain, P. Razavi, B. O'Neill, A. Blake, M. White, A. M. Kelleher, B. McCarthy, R. Murphy, *Nat. Nanotechnol.* **2010**, *5*, 225.
[5] C. M. Lieber, *MRS Bull.* **2011**, *36*, 1052.
[6] B. Li, X. H. Cao, H. G. Ong, J. W. Cheah, X. Z. Zhou, Z. Y. Yin, H. Li, J. L. Wang, F. Boey, W. Huang, H. Zhang, *Adv. Mater.* **2010**, *22*, 3058.
[7] X. F. Duan, C. M. Niu, V. Sahi, J. Chen, J. W. Parce, S. Empedocles, J. L. Goldman, *Nature* **2003**, *425*, 274.
[8] M. S. Gudiksen, L. J. Lauhon, J. Wang, D. C. Smith, C. M. Lieber, *Nature* **2002**, *415*, 617.
[9] X. F. Duan, Y. Huang, Y. Cui, J. F. Wang, C. M. Lieber, *Nature* **2001**, *409*, 66.
[10] L. Liao, Z. Zhang, B. Yan, Z. Zheng, Q. L. Bao, T. Wu, C. M. Li, Z. X. Shen, J. X. Zhang, H. Gong, J. C. Li, T. Yu, *Nanotechnology* **2009**, *20*, 085203.
[11] Y. L. Cao, Y. B. Tang, Y. Liu, Z. T. Liu, L. B. Luo, Z. B. He, J. S. Jie, R. Vellaisamy, W. J. Zhang, C. S. Lee, S. T. Lee, *Nanotechnology* **2009**, *20*, 455705.
[12] B. Xiang, P. W. Wang, X. Z. Zhang, S. A. Dayeh, D. P. R. Aplin, C. Soci, D. P. Yu, D. L. Wang, *Nano Lett.* **2007**, *7*, 323.
[13] Y. B. Tang, X. H. Bo, J. Xu, Y. L. Cao, Z. H. Chen, H. S. Song, C. P. Liu, T. F. Hung, W. J. Zhang, H. M. Cheng, I. Bello, S. T. Lee, C. S. Lee, *ACS Nano* **2011**, *5*, 3591.
[14] F. Sauvage, V. Bodenez, J. M. Tarascon, K. R. Poeppelmeier, *J. Am. Chem. Soc.* **2010**, *132*, 6778.
[15] J. M. Song, Y. Z. Lin, H. B. Yao, F. J. Fan, X. G. Li, S. H. Yu, *ACS Nano* **2009**, *3*, 653.
[16] C. R. Xiong, A. E. Aliev, B. Gnade, K. J. Balkus Jr., *ACS Nano* **2008**, *2*, 293.
[17] S. J. Bao, Q. L. Bao, C. M. Li, T. P. Chen, C. Q. Sun, Z. L. Dong, Y. Gan, J. Zhang, *Small* **2007**, *3*, 1174.
[18] H. S. Lin, P. A. Maggard, *Inorg. Chem.* **2008**, *47*, 8044.
[19] R. Konta, H. Kato, H. Kobayashi, A. Kudo, *Phys. Chem. Chem. Phys.* **2003**, *5*, 3061.
[20] M. W. Shao, L. Lu, H. Wang, S. Wang, M. L. Zhang, D. D. D. Ma, S. T. Lee, *Chem. Commun.* **2008**, 2310.
[21] M. I. Bertoni, N. J. Kidner, T. O. Mason, T. A. Albrecht, E. M. Sorensen, K. R. Poeppelmeier, *J. Electroceram.* **2007**, *18*, 189.
[22] G. Nagaraju, G. T. Chandrappa, J. Livage, *Bull. Mater. Sci.* **2008**, *31*, 367.

© 2013 WILEY-VCH Verlag GmbH & Co. KGaA, Weinheim

[23] S. S. Sunu, V. Jayaraman, E. Prabhu, K. I. Gnanasekar, T. Gnanasekaran, *Ionics* **2004**, *10*, 244.
[24] S. Y. Zhang, W. Y. Li, C. S. Li, J. Chen, *J. Phys. Chem. B* **2006**, *110*, 24855.
[25] W. F. Jin, Y. Ye, L. Gan, B. Yu, P. C. Wu, Y. Dai, H. Meng, X. F. Guo, L. Dai, *J. Mater. Chem.* **2012**, *22*, 2863.
[26] C. C. Chen, M. Aykol, C. C. Chang, A. F. J. Levi, S. B. Cronin, *Nano Lett.* **2011**, *11*, 1863.
[27] P. Wadhwa, B. Liu, M. A. McCarthy, Z. C. Wu, A. G. Rinzler, *Nano Lett.* **2010**, *10*, 5001.
[28] Y. Jiang, W. J. Zhang, J. S. Jie, X. M. Meng, X. Fan, S.-T. Lee, *Adv. Funct. Mater.* **2007**, *17*, 1795.
[29] E. M. Sorensen, H. K. Izumi, J. T. Vaughey, C. L. Stern, K. R. Poeppelmeier, *J. Am. Chem. Soc.* **2005**, *127*, 6347.
[30] M. S. Whittingham, *Chem. Rev.* **2004**, *104*, 4271.
[31] L. Mai, L. Xu, Q. Gao, C. Han, B. Hu, Y. Pi, *Nano Lett.* **2010**, *10*, 2604.
[32] D. T. Schoen, C. Xie, Y. Cui, *J. Am. Chem. Soc.* **2007**, *129*, 4116.
[33] X. G. Bai, H. D. Liu, D. C. McIntosh, J. C. Campbell, *IEEE J. Quantum Electron.* **2009**, *45*, 300.
[34] S. H. Lee, G. Jo, W. Park, S. Lee, Y. S. Kim, B. K. Cho, T. Lee, W. B. Kim, *ACS Nano* **2010**, *4*, 1829.
[35] E. Stern, J. F. Klemic, D. A. Routenberg, P. N. Wyrembak, D. B. Turner Evans, A. D. Hamilton, D. A. LaVan, T. M. Fahmy, M. A. Reed, *Nature* **2007**, *445*, 519.
[36] N. Elfstrom, R. Juhasz, I. Sychugov, T. Engfeldt, A. E. Karlstrom, J. Linnros, *Nano Lett.* **2007**, *7*, 2608.
[37] Z. Y. Fan, J. G. Lu, *IEEE Trans. Nanotechnol.* **2006**, *5*, 393.
[38] P. R. Nair, M. A. Alam, *IEEE Trans. Electron Devices* **2007**, *54*, 3400.
[39] S. M. Bergin, Y. H. Chen, A. R. Rathmell, P. Charbonneau, Z. Y. Li, B. J. Wiley, *Nanoscale* **2012**, *4*, 1996.
[40] S. Barth, M. M. Kolesnik, K. Donegan, V. Krstic, J. D. Holmes, *Chem. Mater.* **2011**, *23*, 3335.
[41] G. Gruner, *Anal. Bioanal.Chem.* **2006**, *384*, 322.
[42] D. H. Zhang, Z. Q. Liu, C. Li, T. Tang, X. L. Liu, S. Han, B. Lei, C. W. Zhou, *Nano Lett.* **2004**, *4*, 1919.
[43] J. Wallentin, M. Ek, L. R. Wallenberg, L. Samuelson, M. T. Borgstrom, *Nano Lett.* **2012**, *12*, 151.
[44] W. K. Hong, G. Jo, J. I. Sohn, W. Park, M. Choe, G. Wang, Y. H. Kahng, M. E. Welland, T. Lee, *ACS Nano* **2010**, *4*, 811.
[45] C. Y. Chen, J. R. D. Retamal, I. W. Wu, D. H. Lien, M. W. Chen, Y. Ding, Y. L. Chueh, C. I. Wu, J. H. He, *ACS Nano* **2012**, *6*, 9366.
[46] L. B. Luo, X. B. Yang, F. X. Liang, H. Xu, Y. Zhao, X. Xie, W. F. Zhang, S. T. Lee, *J. Phys. Chem. C* **2011**, *115*, 18453.
[47] H. Takagi, H. Y. Hwang, *Science* **2010**, *327*, 1601.
[48] Y. Han, R. Lupitskyy, T. M. Chou, C. M. Stafford, H. Du, S. Sukhishvili, *Anal. Chem.* **2011**, *83*, 5873.
[49] C. N. Lok, C. M. Ho, R. Chen, Q. Y. He, W. Y. Yu, H. Z. Sun, P. K. H. Tam, J. F. Chiu, C. M. Che, *J. Biol. Inorg. Chem.* **2007**, *12*, 527.

© 2013 WILEY-VCH Verlag GmbH & Co. KGaA, Weinheim